g values of effective mass donors in $Al_xGa_{1-x}N$ alloys

M. W. Bayerl, M. S. Brandt,* T. Graf, O. Ambacher, J. A. Majewski, and M. Stutzmann

Walter Schottky Institut, Technische Universität München, Am Coulombwall, D-85748 Garching, Germany

D. J. As and K. Lischka

Universität Paderborn, Fachbereich Physik, Warburger Straße 100, D-33095 Paderborn, Germany

Electron spin resonance experiments were performed on Si-doped wurtzite and zinc-blende GaN and Si-doped wurtzite $Al_xGa_{1-x}N$ alloys with $x = 0.15$, 0.32, 0.52, 0.75, and 1. For zinc-blende GaN, an isotropic g factor of 1.9475 is found. The g tensors of the silicon effective mass donor in wurtzite GaN and $Al_xGa_{1-x}N$ alloys are determined experimentally, and for $x < 0.38$ are identical within experimental error to tensors observed in unintentionally n-type-doped material. With increasing Al content, the g values increase and the g-tensor anisotropy is reduced. The g values are calculated within a five-band $k \cdot p$ model in the cubic approximation. To account for the isotropic g factor of wurtzite AlN, a nonvanishing spin-orbit coupling of the higher Γ_5 conduction bands of the order of 50 meV is necessary. To describe the anisotropy at lower Al content, a full seven-band $k \cdot p$ model for the wurtzite crystal structure is investigated. The model shows that the anisotropy in this material system is also due to coupling to higher conduction bands rather than to valence bands. Additional estimates for the momentum matrix elements and the interband mixing coefficients are discussed.

I. INTRODUCTION

The $k \cdot p$ theory has proved to be an important tool for the modeling of physical properties of semiconductors. It has been successfully applied, for example, for band-structure calculations and the determination of effective masses and g values in many semiconducting materials. Initial work on InSb,[1] and on the elementary group-IV semiconductors silicon and germanium,[2–4] was soon extended to various III-V and II-VI compound semiconductors[5] as well. Later on, the effects of alloying in III-V compounds[6] were added to these studies. As most semiconductors of interest crystallize in the cubic zinc-blende phase, the vast majority of the calculations have been performed using this crystal structure. The high symmetry of the cubic system leads to a comparatively small number of parameters that can describe the band structure of the material at the Γ point: the energy gaps E_0 and E_0', the spin-orbit-splitting constants Δ_0 and Δ_0', and the momentum matrix elements P and P'. As is conventional, the primed symbols refer to properties of higher conduction bands, while the others describe properties of the valence bands. The measurement and identification of the influence of each parameter on the effective mass or the g factor is quite obvious because of the small number of parameters.

For wurtzite-type crystals, the situation is more complex, since due to the lower symmetry a larger number of parameters is necessary for an exact treatment. Calculations of valence-band parameters such as splitting constants and interband mixing coefficients[7] and a correct treatment of the effective mass tensor are already well established for the wurtzite symmetry. On the other hand, the situation for the modeling of the g factors is different. Here, wurtzite-type materials, such as CdSe and GaN, have been described only in the cubic approximation, partly due to the nonavailability of various of the band-structure parameters.

Group-III nitrides have recently been subject to intense investigation, primarily motivated by the successful use of this material system in light-emitting diodes, lasers, and high-frequency transistors. However, many details of the band structure of the wurtzite group-III nitrides are still not well known, e.g., basic band-structure parameters of the higher conduction bands in GaN. In this paper, we study the g factor of conduction-band electrons in the $Al_xGa_{1-x}N$ system, using conventional electron-spin resonance (ESR) to determine the g factor experimentally over the whole composition range and $k \cdot p$ theory to extract band-structure information from these data. While the electron g values of most semiconductors and in particular of the other III-V compounds are dominated by the contributions of the valence bands, we find that in the $Al_xGa_{1-x}N$ system the large band gap in combination with the quite small valence-band splitting energies cause a reduction of the valence-band influence. Rather, contributions of coupling to the higher conduction bands are found to be very important. A second characteristic of the wurtzite $Al_xGa_{1-x}N$ system is the anisotropy of the g values due to the hexagonal symmetry. In order to allow modeling of this anisotropy, we have derived the components of the wurtzite g tensor in a seven-band model, and discuss values for the band-structure parameters in GaN and AlN that are compatible with the experimental observations.

It is commonly known that electrons bound to effective mass donors show roughly the same g values as free conduction-band electrons.[8] In the case of GaN, the "native" shallow defect observed in nominally undoped material has been used to investigate the g factor of conduction-band electrons, using a cubic five-band $k \cdot p$ model to extract band-structure information. However, oxygen, which is now considered to cause this unintentional doping, quickly forms a deep state with increasing Al content x in $Al_xGa_{1-x}N$, and therefore this method is not suitable for such studies for $x > 0.4$. In contrast, Si is the donor with the lowest binding energy in GaN and, although exhibiting a *DX*-like behavior

at higher Al concentration, it can be optically excited into its effective-mass-like paramagnetic state also for those alloys.[9] Therefore, we here use the Si donor as the probe best suited for determination of the g values of conduction-band electrons in $Al_xGa_{1-x}N$ alloys.

II. EXPERIMENT

A set of six wurtzite $Al_xGa_{1-x}N$ samples with approximate aluminum content x of 0, 0.15, 0.32, 0.52, 0.75, and 1 and a zinc-blende GaN film were investigated. The wurtzite and zinc-blende samples, with typical thicknesses of 1 μm, were grown by plasma-induced molecular-beam epitaxy on c-plane sapphire and (001) GaAs substrates, respectively, and intentionally doped with Si in the range of 1×10^{18} to 1×10^{19} cm^{-3}. Further details of the growth are given elsewhere.[10–12] The aluminum content of the $Al_xGa_{1-x}N$ alloys was determined with high-resolution x-ray diffraction by measurements of the symmetric (002) and the asymmetric (205) reflexes. Via the position of the asymmetric reflex the Al content is corrected for effects of strain due to varying layer thicknesses and doping concentrations. The ESR experiments were performed in a standard 9.3 GHz Bruker 300 ESP spectrometer using a 6 in. pole-face electromagnet with a maximum field of 1.1 T. The temperature could be varied between 4 and 300 K using a liquid-helium flow cryostat. The samples could be illuminated inside the cryostat using a tungsten lamp and additional band-pass filters, when monochromatic light was required for spectrally resolved studies on the *DX* behavior of $Al_xGa_{1-x}N$ layers with high Al content.

III. ESR RESULTS

The ESR spectra of the Si-doped zinc-blende GaN and the wurtzite $Al_xGa_{1-x}N$ alloys are summarized in Fig. 1. While the g value of the zinc-blende sample ($g_{\parallel} = g_{\perp} = 1.9475$) is slightly smaller than the value published previously for nominally undoped *n*-type material ($g_{\parallel} = g_{\perp} = 1.9533$),[13,14] the g values and anisotropy of the wurtzite GaN layer match the values published by Carlos *et al.*[15] for the intrinsic shallow donor in wurtzite GaN. The results for the alloys with 15% and 32% Al agree with previous reports on unintentionally *n*-type-doped material as well.[16–18] However, this agreement cannot be used to chemically identify the residual donor in GaN and $Al_xGa_{1-x}N$ with Si. As long as both donors are shallow enough to be considered as effective-mass-like states, they will have almost identical g values according to effective mass theory, at least within the accuracy of 9 GHz ESR.

A summary of the g factors found for the $Al_xGa_{1-x}N$ samples studied here is given in Table I. There are two apparent trends correlated with the Al mole fraction: The g values increase with increasing Al content, while the anisotropy simultaneously decreases.

As a function of temperature, all layers exhibit an initial decrease in linewidth before the ESR line starts to broaden. This is shown exemplarily for an AlN:Si sample in Fig. 2. Such a temperature dependence has already been observed in
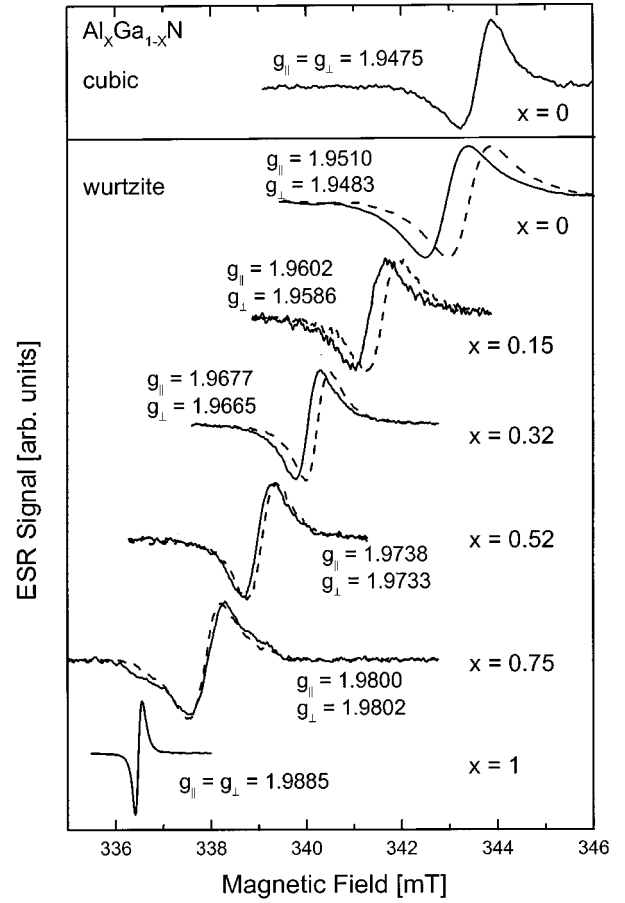
FIG. 1. ESR spectra of silicon-doped zinc-blende GaN and wurtzite $Al_xGa_{1-x}N$ samples. The full lines show the spectra for orientation of the magnetic field parallel to the c axis of the wurtzite epilayers, the dashed lines for orientation perpendicular to the c axis. With increasing Al mole fraction x the g factor increases, whereas the g-factor anisotropy of the wurtzite crystals is reduced.

i-GaN.[15] The initial decrease in linewidth was attributed to motional narrowing due to electron hopping between neighboring donor sites, leading to an increased averaging of inhomogeneous hyperfine broadening. The broadening observed at higher temperatures is caused by a reduction of the spin lifetime[19] as a result of electron-phonon scattering.

The samples with 75% and 100% Al additionally exhibit clear *DX*-like behavior of the Si donors.[9] The *DX* assignment

TABLE I. Compilation of g values for silicon-doped zinc-blende and wurtzite $Al_xGa_{1-x}N$ samples.

Al content x	$g_{\parallel}$	$g_{\perp}$	Crystal structure
0	1.9475		zinc blende
0	1.9510	1.9483	wurtzite
0.15	1.9602	1.9586	wurtzite
0.32	1.9677	1.9665	wurtzite
0.52	1.9738	1.9733	wurtzite
0.75	1.9800	1.9802	wurtzite
1	1.9885		wurtzite
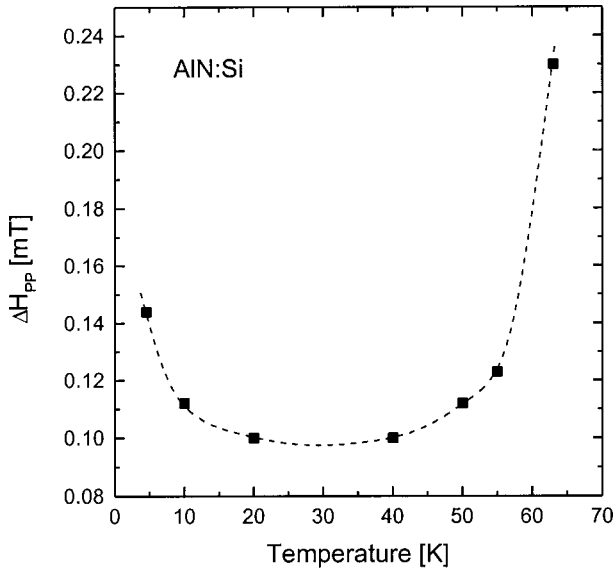
FIG. 2. Temperature dependence of the peak-to-peak electron-spin resonance linewidth of effective mass donors in AlN:Si. The dashed line is a guide to the eye.

is based on the following experimental observations. At room temperature no ESR signal can be detected. After cooling the samples in the dark, the samples are highly resistive and still no ESR signal can be observed. However, upon illumination with photon energies larger than 1.3 and 1.5 eV for the $Al_{0.75}Ga_{0.25}N$ and AlN layers, respectively, the samples become conductive and simultaneously an ESR signal appears (cf. Fig. 3). Both the conductivity and the ESR signal persist after switching off the light. Finally, the ESR signal as well as the persistent photoconductivity simultaneously vanish above 60 K. These phenomena indicate that the neutral, paramagnetic Si donor d^0 in both samples can
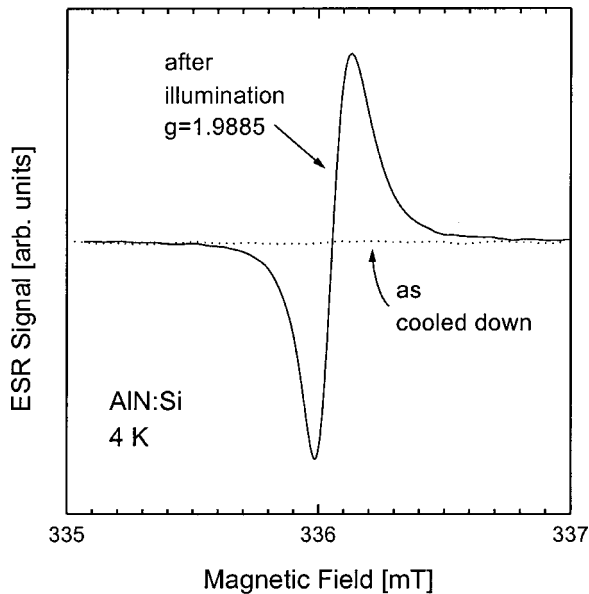
FIG. 3. Comparison of the electron-spin resonance observed in AlN:Si after cooling the sample to 4 K in the dark and after subsequent illumination. The light-induced resonance persists in the dark.

minimize its energy by undergoing a structural relaxation and binding a second electron, hence forming a deep, diamagnetic DX^- state ($2d^0 \rightarrow DX^- + d^+$). Such behavior is well known in the $Al_xGa_{1-x}As$ material system.[20–22] Due to the DX reaction, the shallow effective-mass-like d^0 state of substitutional Si is metastable; however, it can be stabilized at low temperatures due to an energetic barrier for the d^0 to DX transition. The spectra shown here for alloys with high Al concentration therefore show the same paramagnetic state of the Si donor as do the alloys with low Al concentration.

Finally, note that the width of the spin resonance line of the AlN sample in Fig. 1 is significantly smaller than the linewidth for the other samples. This implies that either the spin relaxation time is much longer when Ga is absent or the motional narrowing which is found to influence the linewidth is much stronger in this material.

IV. MODELING OF THE *g* VALUES

A. $Al_xGa_{1-x}N$ alloys in cubic approximation

In previous publications, the effective mass approximation in a cubic five-band $k \cdot p$ model was used to calculate the *g* values of electrons in zinc-blende GaN,[13] wurtzite GaN and $Al_xGa_{1-x}N$ alloys with aluminum content of up to 30%,[15] and wurtzite $In_xGa_{1-x}N$ alloys.[23] In this model, the *g* value and the effective mass of conduction-band electrons are given by[24,25]

$$\frac{g_c}{g_0} - 1 = -\frac{P^2}{3}\left[\frac{\Delta_0}{E_0^2} + \lambda^2 \frac{\Delta_0'}{(E_0' - E_0)^2}\right], \quad (1)$$

$$\frac{m_0}{m^*} - 1 = P^2\left[\frac{1}{E_0} - \frac{\lambda^2}{E_0' - E_0}\right]. \quad (2)$$

Here g_c and m^* denote the *g* value and effective mass of electrons in the conduction band, whereas g_0 and m_0 are the free-electron values. E_0 and $E_0' - E_0$ are the band separations between the Γ_1 conduction band and the Γ_5 valence and conduction bands (cf. Fig. 4), which are coupled by the matrix elements P^2 and $P'^2 = \lambda^2 P^2$, respectively. The Γ_5 valence and conduction bands are spin-orbit split by Δ_0 and Δ_0', respectively. The schematic band structure at the Γ point for cubic zinc-blende symmetry is summarized in Fig. 4.

The cubic approximation seems to be an appropriate first approach for a modeling of the *g* values of pure GaN, since the difference between the *g* values in the zinc-blende ($g_\parallel = g_\perp = 1.9475$) and the wurtzite ($g_\parallel = 1.9510$ and $g_\perp = 1.9483$) GaN is small, and anisotropy effects, which are neglected in this model, are indeed small in wurtzite GaN. Taking experimental values for the energy gap E_0, the spin-orbit splitting Δ_0, and $E_0' - E_0$,[26] and an effective mass of $m^* = 0.2m_0$, the other band parameters were estimated by Carlos *et al.*[15] using Eq. (2). Thus, the parameters λ^2, P^2, and Δ_0' have been restricted to ranges of $0.46 < \lambda^2 < 0.6$, $17\,\text{eV} < P^2 < 23\,\text{eV}$, and $0.1\,\text{eV} < \Delta_0' < 0.3\,\text{eV}$ for GaN.

For modeling the *g* values of the $Al_xGa_{1-x}N$ alloys, the following assumptions were made by Carlos.[16] The gap E_0 was calculated as a function of the Al content using the qua-
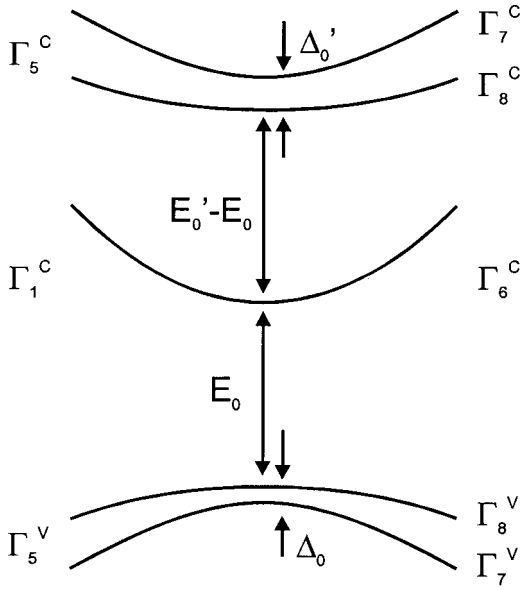
FIG. 4. Schematic picture of the band structure of a cubic $Al_xGa_{1-x}N$ crystal at the Γ point in Koster notation. Here, the v and c superscripts denote functions that form valence and conduction bands, respectively. The transformation properties for the full Bloch functions shown on the right side directly follow from the irreducible representation of the T_d single group shown on the left side when the electronic spin is included into the group-theoretical considerations.

FIG. 5. Fit of the dependence of the g factor of the effective mass donors in $Al_xGa_{1-x}N$ as a function of the Al mole fraction x using the cubic five-band $k \cdot p$ model (1) to the experimental data of Carlos (Ref. 16) and Reinacher *et al.* (Ref. 18) on nominally undoped material and to the experimental data from Si-doped material reported in this work. The dashed line represents a fit with the parameters used by Carlos, assuming zero spin-orbit splitting Δ_0' of the higher conduction bands. The g factor in AlN can be modeled only if a finite value of Δ_0' is taken into account (solid line).

dratic formula which takes into account the experimentally observed bowing. The coupling parameters P^2 and λ^2 and the valence-band spin-orbit splitting Δ_0 were kept constant. The only parameter that was allowed to vary was the spin-orbit splitting Δ_0' of the Γ_5 conduction band, as this splitting is primarily due to the cation, giving large splittings for heavy ions and small for light ions. The magnitude of Δ_0' was linearly varied from the GaN value [$\Delta_0' = 0.25$ eV (Ref. 16)] to zero for AlN. These assumptions give a quite good agreement with the experimental data for $Al_xGa_{1-x}N$ alloys with an Al content below 30%, but the extrapolated value for an electron in the conduction band of AlN is very close to the free-electron value $g = 2.0023$ rather than to the experimentally observed $g = 1.9885$.

Therefore, the present experimental data, covering the whole composition range of the $Al_xGa_{1-x}N$ alloys, make it necessary to reconsider this first analysis. To account for the g value of 1.9885 in AlN, at least a nonvanishing spin-orbit

splitting Δ_0' of the Γ_5 conduction band is necessary. As a crude estimate, Δ_0' should be of the order of 50 meV or even larger in AlN in order to explain the observed g value. But just including a linear variation of Δ_0' in the cubic model presented above still would not fit the experimental data satisfactorily. Under the assumptions mentioned above, the Δ_0' term dominates the predicted g-value dependence on the Al content, which consequently would also be almost linear. The experimentally observed bowing of the g factor can be modeled only if a bowing for Δ_0' is introduced as well, or if the variation of an additional parameter, for example of the coupling constant λ^2, is allowed. We have considered all these arguments and restrictions in order to obtain a reasonable fit to the experimental data of Carlos,[16] Reinacher *et al.*,[18] and this work, which are presented in Fig. 5. The fit was achieved by adjusting the values for λ^2 and Δ_0' to match an average g value $\langle g \rangle = (2g_\perp + g_\parallel)/3$,[4] using Eq. (1) and the effective mass given in Eq. (2) simultaneously. In doing this, some of the values used by Carlos[16] have been replaced with newer experimental and theoretical results. The parameters used for this fit are summarized in Table II. We have used a value of $0.21 m_0$ for the bare effective mass m^*,[27,28] which

TABLE II. Compilation of the parameters used for the five-band fit in Fig. 5 (solid line) of effective mass electron g factors in $Al_xGa_{1-x}N$ alloys. Note that the effective masses are bare band masses excluding polaron effects.

	E_0 (eV)	$E_0' - E_0$ (eV)	Δ_0 (meV)	Δ_0' (meV)	P^2 (eV)	λ^2	m^*/m_0
GaN	3.5	6.5	17	590	15.4	0.27	0.21
AlN	6.2	6.5	14	200	15.4	0.19	0.33

excludes effects due to the formation of polarons leading to heavier effective masses observed in transport experiments, 15.4 eV for the momentum matrix element P^2,[29] and 6.5 eV for the energy gap between the conduction bands[30] $E_0' - E_0$ of GaN taken from more recent experiments.[31] In zinc-blende GaN, the splitting $\Delta_0 \approx 17$ meV of the valence band is due to spin-orbit interaction.[32] For wurtzite GaN, an identical value for the spin-orbit splitting can be derived from optical data[33,34] using Hopfield's quasicubic approximation.[35] In wurtzite GaN, in addition to the spin-orbit interaction, the valence bands are affected by a crystal-field splitting of 11 meV; however, this term is not considered in the cubic five-band $k \cdot p$ model. Also note that the spin-orbit and crystal-field splitting energies in the literature sometimes are assigned the other way round,[36,37] which contradicts the experimental results for zinc-blende GaN. The values for Δ_0 and the bare effective mass m^* of AlN were taken from theory.[38]

We emphasize that this set of parameters should be seen only as an example, as similarly good fits can be achieved within the whole allowed parameter range. For example, an increase of the effective mass would lead to an increase of λ^2 and a reduction of Δ_0'. Indeed, using the polaron mass $0.23m_0$ instead of the bare mass, we would obtain $\lambda^2 = 0.44$ and $\Delta_0' = 340$ meV for GaN. A variation of $E_0' - E_0$, Δ_0, or P^2, in principle, would be compensated in a similar way.

B. The electron g value in zinc-blende GaN

As already mentioned above, we have determined a g factor of 1.9475 for Si donors in zinc-blende GaN. The observed difference from the previously published value of 1.9533 obtained from autodoped material[13] is far beyond the experimental error and therefore has to be related to the nature of the residual donor in zinc-blende GaN, which was assigned to the nitrogen vacancy by Fanciulli, Lei, and Moustakas.[13] This could indicate that the residual donor in nominally undoped material does not completely reflect the properties of conduction-band electrons in zinc-blende GaN, probably due to a larger binding energy. This leads to a stronger localization of the electron on the donor and, therefore, larger central-cell corrections have to be considered. As a consequence, the deviation from the g value of conduction-band electrons will increase and the g factor of such deeper donors will be closer to the free-electron value. It is therefore plausible that the g factor observed in intentionally Si-doped material of $g = 1.9475$ is closer to the g factor of effective mass electrons in zinc-blende GaN. In principle, most of the parameters used to fit the average g factor $\langle g \rangle = (2g_\perp + g_\parallel)/3$ of wurtzite GaN should have almost identical values in zinc-blende GaN. Therefore, to describe the observed value in zinc-blende material, we use the same fit parameters, except for the electronic band gap E_0, which has been experimentally determined to be 3.3 eV in zinc-blende GaN.[32,39] The calculated value for the g factor in the five-
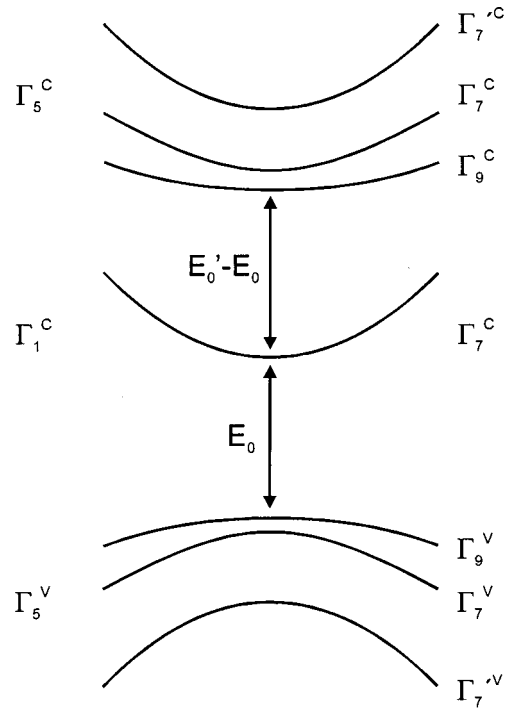
FIG. 6. Schematic picture of the band structure of wurtzite semiconductors at the Γ point. Again, the irreducible representations shown on the right side directly follow from the irreducible representation of the wurtzite C_{6v}^4 single group shown on the left side when the electronic spin is included into the group-theoretical considerations.

band model [Eq. (1)] is then equal to 1.9465, which is extremely close to the value of $g = 1.9475$ observed here, hence confirming our assumptions.

C. Exact treatment of the wurtzite symmetry

The cubic approximation of course cannot account for the anisotropy observed in the wurtzite $Al_xGa_{1-x}N$ alloys. In order to include anisotropy effects, at least the correct wurtzite band structure of the valence band at the Γ point (Fig. 6) has to be included in the $k \cdot p$ calculations. In contrast to the cubic case, here the degeneracy of the light- and heavy-hole bands is lifted due to the crystal-field-splitting term. In wurtzite GaN, the highest valence band is the Γ_9 heavy-hole band followed by the Γ_7 light-hole and the Γ_7 split-off bands (Γ_7').[38] The complete band structure of wurtzite semiconductors at the Γ point is much more complex than shown in Fig. 6.[7] However, due to transition selection rules and the considerably smaller influence of bands with increasing energetic separation, the seven bands presented in Fig. 6 will dominate the properties of conduction-band electrons. In the following, we will derive the g factors for the wurtzite structure in such a seven-band $k \cdot p$ model. For this purpose, we will first consider the valence bands and the lowest conduction band only and later include the effects due to the upper conduction

bands. We will use the set of eight orthonormal base functions near the zone center from Chuang and Chang[40]

$$
\begin{array}{cc}
\text{spin up} & \text{spin down} \\
\end{array}
$$

$$
|iS\uparrow\rangle \qquad\qquad |iS\downarrow\rangle
$$

$$
u_1 = \left| -\frac{X+iY}{\sqrt{2}}\uparrow \right\rangle \qquad u_4 = \left| \frac{X-iY}{\sqrt{2}}\downarrow \right\rangle
$$

$$
u_2 = \left| \frac{X-iY}{\sqrt{2}}\uparrow \right\rangle \qquad u_5 = \left| -\frac{X+iY}{\sqrt{2}}\downarrow \right\rangle \qquad (3)
$$

$$
u_3 = |Z\uparrow\rangle \qquad\qquad u_6 = |Z\downarrow\rangle
$$

Here, the S functions transform like atomic s orbitals, while X, Y, and Z transform like atomic p orbitals oriented along the x, y, and z directions, where z is parallel to the wurtzite crystal's c axis. The $\uparrow$ and $\downarrow$ arrows denote the ''up'' and ''down'' spin eigenstates, respectively.

The solution of the Schrödinger equation

$$
\left(\mathcal{H}_0 + \frac{\hbar^2 k^2}{2m_0} + \frac{\hbar}{m_0}\mathbf{k}\cdot\mathbf{p} + \mathcal{H}_{\text{so}} \right) u_{nk}(\mathbf{r}) = E_n(\mathbf{k})u_{nk}(\mathbf{r}) \quad (4)
$$

in the $k\cdot p$ approximation, including the spin-orbit interaction Hamiltonian, $\mathcal{H}_{\text{so}}$, for the periodic part $u_{nk}(\mathbf{r})$ of the Bloch functions yields the following doubly degenerate eigenvectors for the conduction band and the three valence bands:

$$
\begin{array}{ccc}
\Gamma_7^c & |iS\uparrow\rangle & |iS\downarrow\rangle \\
\Gamma_9^v & u_1 & u_4 \\
\Gamma_7^v & au_2 + bu_6 & bu_3 + au_5 \\
\Gamma_{7'}^v & bu_2 - au_6 & -au_3 + bu_5.
\end{array} \quad (5)
$$

The coupling constants a and b, where $a^2 + b^2 = 1$, introduce a mixing between states with spin-up and spin-down electrons within the Γ_7 valence bands. Therefore, they are often written in the form $a = \sqrt{1-q_7^2}$ and $b = q_7$.[7,41] The corresponding spin mixing can also occur of course between the Γ_9 heavy-hole band and a deeper band of the same symmetry via an equivalent q_9 coupling parameter,[7,42] but this effect is comparatively small due to the large energy separation between the Γ_9 bands and therefore will be neglected here. In the absence of a magnetic field, the eigenvalues of Eq. (4) are spin degenerate and calculated in Refs. 38, 40, and 43 as

$$
E_{\text{CB}}(\Gamma_7^c) = E_0 + \Delta_1 + \Delta_2,
$$

$$
E_1(\Gamma_9^v) = \Delta_1 + \Delta_2,
$$

$$
E_2(\Gamma_7^v) = \frac{\Delta_1 - \Delta_2}{2} + \sqrt{[(\Delta_1-\Delta_2)/2]^2 + 2\Delta_3^2},
$$

$$
E_3(\Gamma_{7'}^v) = \frac{\Delta_1 - \Delta_2}{2} - \sqrt{[(\Delta_1-\Delta_2)/2] + 2\Delta_3^2}, \quad (6)
$$

except for a constant offset, which for convenience was set to zero. Here, in decreasing order of energies, E_{CB} denotes the lowest conduction band, E_1 the heavy-hole, E_2 the light-

TABLE III. Experimentally (expt.) and theoretically (theor.) determined values for the valence-band splitting parameters in GaN.

Δ_1 (meV)	Δ_2 (meV)	Δ_3 (meV)	Reference	
36	5.0	5.9	33	theor.
19	6.3	6.3	33	theor.
24	5.4	6.8	38	theor.
22	5	5	37	expt.
10	6.2	5.5	50	expt.
17	4	4	51	expt.
22	3.7	3.7	36	expt.

hole, and E_3 the crystal-field split-off valence bands. The electronic band gap E_0 is given by the energy difference between the conduction band and the highest valence band, which is the heavy-hole band in GaN. The sequence of the valence bands is predicted to be different for AlN, where the ordering was calculated to be split-off, heavy-hole, and light-hole band.[38]

The Δ_i denote splitting parameters. Using the quasicubic approximation of Hopfield,[35] Δ_1 is usually referred to as the crystal-field splitting, while $\Delta_2 = \Delta_3$ is assigned to $\frac{1}{3}$ of the spin-orbit-splitting energy. Experimental and theoretical values for the Δ_i, as shown in Table III, are also summarized in Ref. 33 or can be derived from the valence-band splittings or the excitonic transition energies given in, e.g., Ref. 34.

It has been shown that the coupling parameters $\sqrt{1-q_7^2}$ and q_7 can be expressed in terms of the band parameters E_2 and Δ_3,[40]

$$
\sqrt{1-q_7^2} = \sqrt{E_2^2/(E_2^2 + 2\Delta_3^2)},
$$

$$
q_7^2 = \frac{2\Delta_3^2}{E_2^2 + 2\Delta_3^2}. \quad (7)
$$

Until this point we have used the nomenclature conventions of Chuang and Chang.[40] Let us now consider the momentum matrix element P, also called the Kane parameter, which in the cubic model described above is given by an isotropic constant. Due to the wurtzite symmetry of the crystal this isotropy is broken and we obtain, in principle, different values for P along and perpendicular to the c axis. For convenience, we define two independent Kane parameters[44] as

$$
P_1 = \sqrt{2/m_0}\langle iS|p_z|Z\rangle,
$$

$$
P_2 = \sqrt{2/m_0}\langle iS|p_x|X\rangle = \sqrt{2/m_0}\langle iS|p_y|Y\rangle, \quad (8)
$$

again with the z direction parallel to the crystallographic c axis. Here, the $p_{x,y,z}$ denote the components of the momentum operator in the x, y, and z directions. P_1^2 and P_2^2 have units of energy.

Now we can calculate the g tensor $\overleftrightarrow{g}$ of effective-mass-like electrons in wurtzite crystals from $k\cdot p$ theory. At the Γ point and in first-order perturbation theory, the standard 3×3 $\overleftrightarrow{g}$ tensor is related to the Pauli spin matrices[4] via

$$
\overleftrightarrow{g}\cdot\boldsymbol{\sigma} = g_0(\boldsymbol{\sigma} + \widetilde{\mathbf{G}}), \quad (9)
$$

where $\boldsymbol{\sigma}$ is a vector consisting of the three Pauli spin matrices

$$\vec{\sigma}_x = \begin{pmatrix} 0 & 1 \\ 1 & 0 \end{pmatrix}, \quad \vec{\sigma}_y = \begin{pmatrix} 0 & -i \\ i & 0 \end{pmatrix}, \quad \vec{\sigma}_z = \begin{pmatrix} 1 & 0 \\ 0 & -1 \end{pmatrix}$$

and $\widetilde{\mathbf{G}}$ is a vector whose elements $\vec{\widetilde{G}}_i$ are 2×2 matrices as well. This results in equations of the form

$$g_{xx}\vec{\sigma}_x + g_{xy}\vec{\sigma}_y + g_{xz}\vec{\sigma}_z = g_0\vec{\sigma}_x + g_0 \begin{pmatrix} \widetilde{G}_x^{\uparrow\uparrow} & \widetilde{G}_x^{\uparrow\downarrow} \\ \widetilde{G}_x^{\downarrow\uparrow} & \widetilde{G}_x^{\downarrow\downarrow} \end{pmatrix}, \quad \text{etc.,} \tag{10}$$

which relate the components of the experimentally observable g tensor to the components of $\widetilde{\mathbf{G}}$, which are defined as[3,45]

$$\vec{\widetilde{G}}_i^{\alpha\beta} = \frac{1}{im_0} \sum_{n \neq \mathrm{CB}} \frac{\langle iS\alpha | \mathbf{p} | n \rangle \langle n | \mathbf{p} | iS\beta \rangle}{E_{\mathrm{CB}} - E_n}. \tag{11}$$

Here α and β label $\uparrow$ and $\downarrow$, $\mathbf{p}$ is the momentum operator, and the functions $|n\rangle$ denote the eigenstates solving Eq. (4), except for the lowest Γ_7 conduction band, whose g tensor is to be calculated. These include, of course, the highest valence-band states from Eq. (5), but in principle also lower valence bands and higher conduction bands of a symmetry that allows optical dipole transitions.

For the purpose of illustration, we present the derivation of the $\widetilde{G}_z^{\uparrow\uparrow}$ component, which is defined as

$$\widetilde{G}_z^{\uparrow\uparrow} = \frac{1}{im_0} \sum_{n \neq \mathrm{CB}}$$

$$\times \frac{\langle iS\uparrow | p_x | n \rangle \langle n | p_y | iS\uparrow \rangle - \langle iS\uparrow | p_y | n \rangle \langle n | p_x | iS\uparrow \rangle}{E_{\mathrm{CB}} - E_n}. \tag{12}$$

For the three valence-band states [see Eq. (5)], the evaluation of the matrix elements yields

$$\langle iS\uparrow | p_x | \Gamma_9^\uparrow \rangle = -\frac{\sqrt{m_0}}{2} P_2, \quad \langle iS\uparrow | p_y | \Gamma_9^\uparrow \rangle = -i\frac{\sqrt{m_0}}{2} P_2,$$

$$\langle iS\uparrow | p_x | \Gamma_9^\downarrow \rangle = 0, \quad \langle iS\uparrow | p_y | \Gamma_9^\downarrow \rangle = 0,$$

$$\langle iS\uparrow | p_x | \Gamma_7^\uparrow \rangle = \frac{\sqrt{m_0}}{2} \sqrt{1 - q_7^2} P_2,$$

$$\langle iS\uparrow | p_y | \Gamma_7^\uparrow \rangle = -i\frac{\sqrt{m_0}}{2} \sqrt{1 - q_7^2} P_2,$$

$$\langle iS\uparrow | p_x | \Gamma_7^\downarrow \rangle = 0, \quad \langle iS\uparrow | p_y | \Gamma_7^\downarrow \rangle = 0,$$

$$\langle iS\uparrow | p_x | \Gamma_{7'}^\uparrow \rangle = \frac{\sqrt{m_0}}{2} q_7 P_2, \quad \langle iS\uparrow | p_y | \Gamma_{7'}^\uparrow \rangle = -i\frac{\sqrt{m_0}}{2} q_7 P_2,$$

$$\langle iS\uparrow | p_x | \Gamma_{7'}^\downarrow \rangle = 0, \quad \langle iS\uparrow | p_y | \Gamma_{7'}^\downarrow \rangle = 0, \tag{13}$$

and therefore

$$\widetilde{G}_z^{\uparrow\uparrow} = \frac{P_2^2}{2} \left(-\frac{1}{E_{\mathrm{CB}} - E_1} + \frac{1 - q_7^2}{E_{\mathrm{CB}} - E_2} + \frac{q_7^2}{E_{\mathrm{CB}} - E_3} \right). \tag{14}$$

As we have already seen for zinc-blende crystals, the g values of the $Al_xGa_{1-x}N$ alloys are strongly affected by contributions due to the higher conduction bands via the momentum matrix element P'. In fact, these contributions were shown to even exceed the effects of the valence bands described above. Therefore, we have to include the next higher set of conduction bands of Γ_5 symmetry into the calculations for wurtzite symmetry, too. Contributions of further conduction and valence bands are neglected due to their much smaller effect. Owing to the hexagonal symmetry, the g tensor is axially symmetric:

$$\vec{\vec{g}} = \begin{pmatrix} g_\perp & 0 & 0 \\ 0 & g_\perp & 0 \\ 0 & 0 & g_\parallel \end{pmatrix} \tag{15}$$

and in our full seven-band $k\cdot p$ model the components are

$$\frac{g_\perp}{g_0} - 1 = \frac{P_1 P_2}{2} \left(\frac{1}{E_{\mathrm{CB}} - E_3} - \frac{1}{E_{\mathrm{CB}} - E_2} \right) \sqrt{2q_7^2(1 - q_7^2)}$$

$$+ \frac{P_1' P_2'}{2} \left(\frac{1}{E_{\mathrm{CB}} - E_3'} - \frac{1}{E_{\mathrm{CB}} - E_2'} \right) \sqrt{2q_7'^2(1 - q_7'^2)},$$

$$\frac{g_\parallel}{g_0} - 1 = \frac{P_2^2}{2} \left(-\frac{1}{E_{\mathrm{CB}} - E_1} + \frac{1 - q_7^2}{E_{\mathrm{CB}} - E_2} + \frac{q_7^2}{E_{\mathrm{CB}} - E_3} \right)$$

$$+ \frac{P_2'^2}{2} \left(-\frac{1}{E_{\mathrm{CB}} - E_1'} + \frac{1 - q_7'^2}{E_{\mathrm{CB}} - E_2'} + \frac{q_7'^2}{E_{\mathrm{CB}} - E_3'} \right). \tag{16}$$

Here, primed parameters refer to the higher conduction bands. In contrast to previous treatments of g factors in wurtzite crystals,[41,46] Eq. (16) explicitly includes the higher conduction bands and also takes into account the anisotropy of the momentum matrix elements. For completeness, we also give the results for the effective mass tensor $\vec{\vec{m}}^*$ in this approximation:[41]

$$\frac{m_0}{m_\perp} - 1 = \frac{P_2^2}{2} \left(\frac{1}{E_{\mathrm{CB}} - E_1} + \frac{1 - q_7^2}{E_{\mathrm{CB}} - E_2} + \frac{q_7^2}{E_{\mathrm{CB}} - E_3} \right)$$

$$+ \frac{P_2'^2}{2} \left(\frac{1}{E_{\mathrm{CB}} - E_1'} + \frac{1 - q_7'^2}{E_{\mathrm{CB}} - E_2'} + \frac{q_7'^2}{E_{\mathrm{CB}} - E_3'} \right),$$

$$\frac{m_0}{m_\parallel} - 1 = P_1^2 \left(\frac{q_7^2}{E_{\mathrm{CB}} - E_2} + \frac{1 - q_7^2}{E_{\mathrm{CB}} - E_3} \right)$$

$$+ P_2'^2 \left(\frac{q_7'^2}{E_{\mathrm{CB}} - E_2'} + \frac{1 - q_7'^2}{E_{\mathrm{CB}} - E_3'} \right), \tag{17}$$

which obviously reflects the same symmetry as the g tensor. Note that the contributions of the valence bands and of the

higher conduction bands to Eqs. (16) and (17), in principle, have opposite signs due to the change of sign in the energy denominator.

The better-known Eqs. (1) and (2), resulting from the five-band $k \cdot p$ model used for the description of cubic materials, can be derived from Eqs. (16) and (17) by setting $E_1 = E_2$ (i.e., zero crystal-field splitting), $q_7^2 = \frac{2}{3}$, and $P_1 = P_2$, and using the identical assumptions for the equivalent primed parameters.

Let us now evaluate the experimentally observed values of the effective mass and g tensor of wurtzite GaN and AlN on the basis of Eqs. (16) and (17), postponing the discussion of alloys for a moment. The components of the effective mass tensor (17) are dominated by terms proportional to P_i^2 / E_0 and $P_i'^{\,2} / E_0'$. All other terms are smaller by at least a factor of $\Delta_i / E_0 (< 10^{-2})$ and therefore to first order can be neglected in this evaluation. In addition, while modeling the effective mass in the cubic crystal, we have already seen that the contributions due to the valence bands are larger by more than a factor of 4 compared to the contributions of the higher conduction bands (cf. Table II). For these reasons, we can expect that an anisotropy of the momentum matrix elements P_i will govern the anisotropy of the effective mass tensor as well. However, the anisotropy of the effective masses of conduction-band electrons is found to be small in both GaN and AlN, i.e., $|m_\parallel - m_\perp| < 0.01 m_0$.[38] Therefore, we can estimate the anisotropy of the momentum matrix element to be $|P_1^2 - P_2^2| < 1$ eV, which is in good agreement with theoretical calculations.[47]

Such a small difference between P_1^2 and P_2^2 cannot account for the observed anisotropy of the g factors in wurtzite GaN. If the anisotropy of the g factor of wurtzite GaN is caused by the valence bands, we have to consider the effect resulting from q_7^2, since it is the only free parameter left. As mentioned above, q_7^2 is determined by Eq. (7) and can be calculated for wurtzite GaN using the quasicubic approximation of Hopfield[35] for Eq. (6), and, e.g., experimental values for the valence-band splittings. This approach yields 17.2 ± 1 meV for the spin-orbit splitting and $\Delta_1 = 10.8 \pm 1$ meV for the crystal-field splitting and, thus, $q_7^2 \approx 0.35$.

In addition to the ambiguous assignment of the splitting energies, the value of q_7^2 is also quite sensitive to the validity of the Hopfield approximation, i.e., $\Delta_2 = \Delta_3$. However, according to theory, differences between Δ_2 and Δ_3 of the order of 1 meV seem to be reasonable.[33,38] This would have a considerable influence on the q_7^2 parameter. Therefore, we have to check the validity of the estimated value for q_7^2 by other means.

Another way to look for the proper value of q_7^2 would be determine exactly the intensity ratios of the excitonic transitions along the different crystallographic directions,[7] since q_7^2 is also given by

$$q_7^2 = \frac{1}{1 + f_B^\perp / f_C^\perp} = \frac{1}{1 + f_C^\parallel / f_B^\parallel}, \qquad (18)$$

where f denotes the oscillator strength of the B and C excitons for excitation perpendicular and parallel to the c axis. The work of Gil, Hamdani, and Morkoc[48] would give an
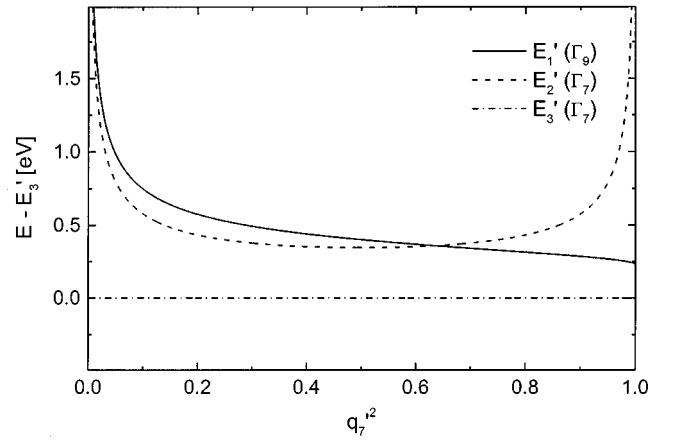
FIG. 7. Dependence of the separations of the higher conduction bands in wurtzite GaN on the appropriate interband mixing parameter $q_7'^{\,2}$. In this plot, the energy scale is referenced to the E_3' higher conduction band.

estimate of $q_7^2 \approx 0.27$ for unstrained GaN, which confirms the assignment of 17 meV to the spin-orbit splitting suggested above.

The situation with respect to the q_7^2 parameter is even more uncertain for AlN than for GaN. The only information available today on the valence-band structure is from theory. Here, an ordering of the bands with $E(\Gamma_7') > E(\Gamma_9) > E(\Gamma_7)$ is predicted with a separation of about 220 meV between the two Γ_7 bands. This would lead to a q_7^2 value close to 0, reflecting a strongly reduced mixing of the Γ_7 states due to their large energetic separation.

More importantly, when evaluating Eqs. (16) and (17) using an isotropic P^2, which is reasonable according to our considerations above on the effective mass, and experimentally determined values for the other parameters, we find that the measured g-factor anisotropy of wurtzite GaN ($g_\parallel = 1.951$, $g_\perp = 1.9483$) cannot be explained by the valence-band terms in Eq. (16), independent of the actual value of q_7^2. In contrast, the valence-band contributions in Eq. (16) alone would yield an anisotropic effect with the opposite sign, i.e., $g_\parallel < g_\perp$.

Therefore, the anisotropy of the g factor of conduction-band electrons in wurtzite GaN has to be attributed to the set of higher conduction bands. After choosing a value for q_7^2 (we use a value of ≈ 0.35 corresponding to a spin-orbit splitting of 17 meV following the above considerations), the energy splittings of these bands directly ensue from the observed g values as a function of $q_7'^{\,2}$ provided $P'^{\,2}$ is also considered isotropic. In the absence of any theoretical predictions for $P'^{\,2}$, this assumption appears warranted in view of the small anisotropy of the corresponding P^2 discussed above. The calculated dependence of the energies of the upper conduction bands on the $q_7'^{\,2}$ parameter is shown in Fig. 7. Unfortunately, no detailed information on the band structure of the higher conduction bands in GaN is known so far. Therefore, we cannot determine explicit values for the splitting energies and the $q_7'^{\,2}$ parameter from existing experimental data. However, from Fig. 7 we can predict the E_3'
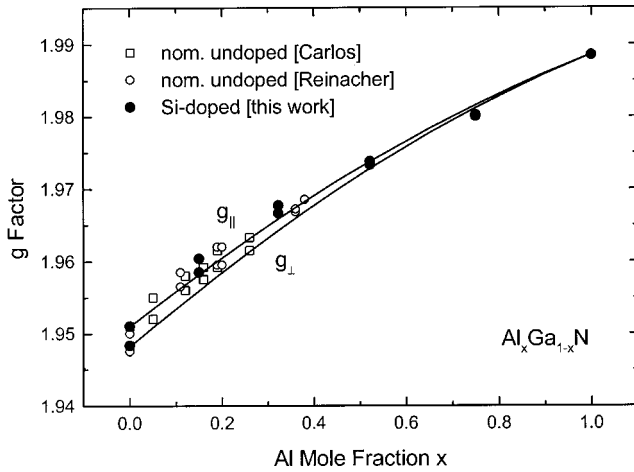
FIG. 8. Seven-band $k \cdot p$ fit of the g factors of wurtzite $Al_xGa_{1-x}N$ as a function of the Al mole fraction x using Eq. (16) and the band-structure parameters discussed in the text.

level to be lower in energy by more than 0.3 eV relative to the E_1' and E_2' bands, independent of the value of $q_7'^2$. Even if measured indirectly, this represents an experimentally determined value for the splittings of the upper conduction bands in GaN and would not be significantly changed by an anisotropy of P'^2 similar to that observed for P^2.

Whereas the majority of the parameters used for the modeling of the g factor of wurtzite GaN are established, most of the parameters for AlN are highly uncertain or even unknown. Therefore, it would be very speculative to derive the corresponding values for the parameters in AlN here. However, with the parameters used in the cubic approximation (1) (cf. Table II) a good agreement with the experimental g values can already be obtained for AlN, since no anisotropy is observed. However, the cubic approximation may lead to a wrong assignment of the band-structure parameters and further work is needed to determine the exact conduction-band structure of AlN.

As a first approach to fitting the g values of the $Al_xGa_{1-x}N$ alloys in the wurtzite model (Fig. 8), we have used the parameters listed in Table II in combination with $q_7^2 = 0.35$, $E_3' - E_2' = -0.36$ eV, $E_2' = E_1'$, and $q_7'^2 = 0.63$ as a possible parameter set for GaN. As a function of the Al mole fraction, the parameters have been linearly interpolated between the values for GaN and AlN, as in the $Al_xGa_{1-x}As$ system.[41] An exception was made for the electronic bandgap energies E_0, which are again described by the quadratic formula accounting for the experimentally observed bowing. A bowing of the splitting constants Δ_i and the momentum matrix elements P^2 and P'^2, which in principle can be introduced by effects of disorder,[24] was not taken into account. However, this might turn out to be useful to improve the quality of the simulation, in particular for Al content between 0 and 0.4, since in this range the fits seem to underestimate the measured g values.

The discussion so far has excluded effects of strain on the g values, but at least for the valence-band splitting param-

eters, and therefore q_7^2 as well, a significant influence has been reported in the literature.[48,49] In contrast, the ESR experiments reported so far on the effective mass donor (both in nominally undoped and in Si-doped material) show virtually no variation of the g values of the effective mass donors, even though a large number of samples with different layer properties, in particular including strain, were investigated. A possible reason for this could be that strain effects are compensated by other band-structure parameters, i.e., q_7^2 and the different Δ_i. On the other hand, unlike in most other semiconductor materials, the valence-band terms in $Al_xGa_{1-x}N$ alloys contribute only less than $\frac{1}{3}$ to the deviation of g from the free-electron value g_0. The major contribution is due to the P'^2 terms resulting from the higher conduction bands, and the separations of these bands could be much less sensitive to the effects of strain than observed for valence bands. However, a systematic study of the effect of strain on the g value of conduction-band electrons in GaN remains to be performed.

V. CONCLUSION

To summarize, we have reported ESR measurements of the g factor of silicon-doped $Al_xGa_{1-x}N$ alloys over the whole composition range. For samples with an Al content up to 32% the g values are consistent with those of the residual effective mass donors of $Al_xGa_{1-x}N$ alloys. With increasing Al content, the deviation from the free-electron g value $g_0 = 2.0023$ and the anisotropy simultaneously decrease, until we observe an isotropic g value of 1.9885 for AlN. Within a five-band $k \cdot p$ calculation in cubic approximation, the g values can be modeled only if a nonvanishing splitting Δ_0' of the Γ_5 conduction bands is taken into account for AlN also. A rough estimate gives a value of $\Delta_0' > 50$ meV. To account for the observed bowing of the g values as well, a variation of the matrix elements P^2 or λ^2 of the valence band with the Al content has to be considered. In order to include the anisotropy of the g factors into the model, a derivation of the g values for the correct wurtzite symmetry of the valence and higher conduction bands was performed using a seven-band $k \cdot p$ model. Thus the anisotropy of P^2 could be estimated to be smaller than approximately 1 eV in both GaN and AlN. Likely values for the interband mixing coefficient q_7^2 are ≈ 0.35 for GaN and ≈ 0 for AlN. The seven-band $k \cdot p$ model clearly shows that the anisotropy of the g values in $Al_xGa_{1-x}N$ alloys is in fact caused by the spin-orbit and crystal-field splittings of the higher conduction bands.

*Email address: martin.brandt@physik.tu-muenchen.de

[1] E. O. Kane, J. Phys. Chem. Solids **1**, 249 (1957).

[2] J. M. Luttinger and W. Kohn, Phys. Rev. **97**, 869 (1955).

[3] H. Hasegawa, Phys. Rev. **118**, 1523 (1960).

[4] L. M. Roth, Phys. Rev. **118**, 1534 (1960).

[5] M. Cardona, J. Phys. Chem. Solids **24**, 1543 (1963).

[6] M. Cardona, in *Semiconductors and Semimetals*, edited by R. K. Willardson and Al. C. Beer (Academic, New York, 1967), Vol. 3, Chap. 5.

[7] E. Gutsche and E. Jahne, Phys. Status Solidi **19**, 823 (1967).

[8] C. F. Young, E. H. Poindexter, G. J. Gerardi, W. L. Warren, and D. J. Keeble, Phys. Rev. B **55**, 16 245 (1997).

[9] R. Zeisel, M. W. Bayerl, S. T. B. Goennenwein, R. Dimitrov, O. Ambacher, M. S. Brandt, and M. Stutzmann, Phys. Rev. B **61**, R16 283 (2000).

[10] H. Angerer, O. Ambacher, R. Dimitrov, Th. Metzger, W. Rieger, and M. Stutzmann, MRS Internet J. Nitride Semicond. Res. **1**, 15 (1996).

[11] D. Schikora, M. Hankeln, D. J. As, K. Lischka, T. Litz, A. Waag, T. Buhrow, and F. Henneberger, Phys. Rev. B **54**, R8381 (1996).

[12] D. J. As, A. Richter, J. Busch, B. Schöttker, M. Lübbers, J. Mimkes, D. Schikora, K. Lischka, W. Kriegseis, W. Burkhardt, and B. K. Meyer, in *GaN and Related Alloys*, edited by R. Feenstra, T. Myers, M. S. Shur, and H. Amano, MRS Symposia Proceedings No. 595 (Materials Research Society, Pittsburgh, in press), p. W3.81.1.

[13] M. Fanciulli, T. Lei, and T. D. Moustakas, Phys. Rev. B **48**, 15 144 (1993).

[14] M. Fanciulli, Physica B **205**, 87 (1995).

[15] W. E. Carlos, J. A. Freitas, Jr., M. Asif Khan, D. T. Olson, and J. N. Kuznia, Phys. Rev. B **48**, 17 878 (1993).

[16] W. E. Carlos, in *Proceedings of the 7th International Conference on Shallow-Level Centers in Semiconductors*, edited by C. A. J. Ammerlaan and B. Pajot (World Scientific, Singapore, 1997), p. 13.

[17] M. Stutzmann, O. Ambacher, A. Cros, M. S. Brandt, H. Angerer, R. Dimitrov, N. M. Reinacher, T. Metzger, R. Höpler, D. Brunner, F. Freudenberg, R. Handschuh, and Ch. Deger, Mater. Sci. Eng. B **50**, 212 (1997).

[18] N. M. Reinacher, H. Angerer, O. Ambacher, M. S. Brandt, and M. Stutzmann, in *III-V Nitrides*, edited by F. A. Ponce, T. D. Maistakas, I. Akasaki, and B. A. Monemar, Mater. Res. Soc. Symp. Proc. No. 449 (Materials Research Society, Pittsburgh, 1997), p. 579.

[19] W. E. Carlos, J. A. Freitas, Jr., M. Asif Khan, D. T. Olson, and J. N. Kuznia, Mater. Sci. Forum **143-147**, 99 (1994).

[20] D. V. Lang and R. A. Logan, Phys. Rev. Lett. **39**, 635 (1977).

[21] D. J. Chadi and K. J. Chang, Phys. Rev. Lett. **61**, 873 (1988).

[22] D. V. Lang, in *Deep Centers in Semiconductors*, edited by S. T. Pantelides (Gordon and Breach, Yverdon, 1992), p. 591.

[23] E. R. Glaser, T. A. Kennedy, W. E. Carlos, P. P. Ruden, and S. Nakamura, Appl. Phys. Lett. **73**, 3123 (1998).

[24] C. Hermann and C. Weisbuch, in *Optical Orientation*, edited by F. Meier and B. P. Zakharchenya (Elsevier, Amsterdam, 1984), p. 463.

[25] D. J. Chadi, A. H. Clark, and R. D. Burnham, Phys. Rev. B **13**, 4466 (1976).

[26] S. Bloom, G. Harbeke, E. Meier, and I. B. Orthenburger, Phys. Status Solidi B **66**, 161 (1974).

[27] M. Drechsler, D. M. Hofmann, B. K. Meyer, T. Detchprohm, H. Amano, and I. Akasaki, Jpn. J. Appl. Phys., Part 2 **34**, L1178 (1995).

[28] S. A. McGill, K. Cao, W. B. Fowler, and G. G. DeLeo, Phys. Rev. B **57**, 8951 (1998).

[29] J. S. Im, A. Mortiz, F. Steuber, V. Härle, F. Scholz, and A. Hangleiter, Appl. Phys. Lett. **70**, 631 (1997).

[30] T. Valla, P. D. Johnson, S. S. Dhesi, K. E. Smith, D. Doppalapudi, T. D. Moustakas, and E. L. Shirley, Phys. Rev. B **59**, 5003 (1999).

[31] P. Perlin, E. Litwin-Staszewska, B. Suchanek, W. Knap, J. Camassel, T. Suski, R. Piotrzowski, I. Grzegory, S. Porowski, E. Kaminska, and J. C. Chervin, Appl. Phys. Lett. **68**, 1114 (1996).

[32] G. Ramirez-Flores, H. Navarro-Cotreras, and A. Lastras-Martinez, Phys. Rev. B **50**, 8433 (1994).

[33] K. Kim, W. R. L. Lambrecht, B. Segall, and M. van Schilfgaarde, Phys. Rev. B **56**, 7363 (1997).

[34] K. Kornitzer, T. Ebner, K. Thonke, R. Sauer, C. Kirchner, V. Schwegler, M. Kamp, M. Leszczynski, I. Grzegory, and S. Porowski, Phys. Rev. B **60**, 1471 (1999).

[35] J. J. Hopfield, J. Phys. Chem. Solids **15**, 97 (1960).

[36] R. Dingle, D. D. Sell, S. E. Stokowski, and M. Ilegems, Phys. Rev. B **4**, 1211 (1971).

[37] S. Chichibu, T. Azuhata, T. Sota, H. Amano, and I. Akasaki, Appl. Phys. Lett. **70**, 2085 (1997).

[38] J. A. Majewski, M. Städele, and P. Vogl, in *III-V Nitrides* (Ref. 18), p. 887.

[39] K. H. Ploog, O. Brandt, H. Yang, J. Menniger, and R. Klann, Solid-State Electron. **41**, 235 (1997).

[40] S. L. Chuang and C. S. Chang, Phys. Rev. B **54**, 2491 (1996).

[41] C. Hermann and C. Weisbuch, Phys. Rev. B **15**, 823 (1977).

[42] L. C. Lew Yan Voon, M. Willatzen, M. Cardona, and N. E. Christensen, Phys. Rev. B **53**, 10 703 (1996).

[43] S.-H. Wei and A. Zunger, Appl. Phys. Lett. **69**, 2719 (1996).

[44] E. O. Kane, J. Phys. Chem. Solids **1**, 82 (1956).

[45] L. M. Roth, B. Lax, and S. Zwerdling, Phys. Rev. **114**, 90 (1959).

[46] T. A. Kennedy, E. R. Glaser, W. E. Carlos, P. P. Ruden, and S. Nakamura, MRS Internet J. Nitride Semicond. Res. **4S1**, G7.4 (1999).

[47] M. Suzuki and T. Uenoyama, Jpn. J. Appl. Phys., Part 1 **35**, 543 (1996).

[48] B. Gil, F. Hamdani, and H. Morkoc, Phys. Rev. B **54**, 7678 (1996).

[49] A. Alemu, B. Gil, M. Julier, and S. Nakamura, Phys. Rev. B **57**, 3761 (1998).

[50] B. Gil, O. Briot, and R. L. Aulombard, Phys. Rev. B **52**, R17 028 (1995).

[51] L. Eckey, L. Podlowski, A. Göldner, A. Hoffmann, I. Broser, B. K. Meyer, D. Volm, T. Streibl, T. Detchprohm, H. Amano, and I. Akasaki, in *Silicon Carbide and Related Materials*, edited by S. Nakashima, H. Matsunami, S. Yoshida, and H. Harima, IOP Conf. Proc. No. 142 (Institute of Physics, London, 1996), p. 943.